Mechanical and Tribological Properties of Al$_2$O$_3$-TiC Composite Fabricated by Spark Plasma Sintering Process with Metallic (Ni, Nb) Binders

Rohit Kumar [1,2], Anil K. Chaubey [2,*], Tapabrata Maity [3] and Konda Gokuldoss Prashanth [4,5,*]

1   Academy of Scientific and Innovative Research (AcSIR), New Delhi 110020, India; rohit.met@gmail.com
2   CSIR-Institute of Minerals and Materials Technology (IMMT), Bhubaneswar 751013, India
3   Department of Materials Physics, Montanuniversitat Leoben, Jahnstraße 12, 8700 Leoben, Austria;
     tapabrata.maity@unileoben.ac.at
4   Department of Manufacturing and Civil Engineering, Norwegian University of Science and Technology,
     Teknologivegen 22, 2815 Gjøvik, Norway
5   Erich Schmid Institute of Materials Science, Austrian Academy of Sciences, Jahnstraße 12,
     A-8700 Leoben, Austria
*   Correspondence: anil.immt@gmail.com or akchaubey@immt.res.in (A.K.C.);
     kgprashanth@gmail.com or prashanth.konda@ntnu.no or Prashanth.kondagokuldoss@oeaw.ac.at (K.G.P.);
     Tel.: +91-6742-237-9204 (A.K.C.); +47-973-646-67 (K.G.P.)

Abstract: Al$_2$O$_3$-10TiC composites were fabricated through the powder metallurgical process (mechanical milling combined with spark plasma sintering) with the addition of Ni/Nb as metallic binders. The effect of binder addition (Ni/Nb) on the processing, microstructure, and mechanical and tribological properties of the bulk-sintered composite samples was investigated. The microstructure of the composite reveals a homogeneous distribution of the TiC particles in the Al$_2$O$_3$ matrix. However, the presence of Ni/Nb was not traceable, owing to the small amounts of Ni/Nb addition. Hardness and density of the composite samples increase with the increasing addition of Nb (up to 2 wt. % Nb). Any further increase in the Nb content (3 wt. %) decreases both the hardness and the wear resistance. However, in case of Ni as binder, both the hardness and wear resistance increases with the increase in the Ni content from 1 wt. % to 3 wt. %. However, the composite samples with Nb as binder show improved hardness and wear resistance compared to the composites with Ni as binder.

Keywords: mechanical properties; spark plasma sintering; microstructure; composites; abrasion test

1. Introduction

Ceramic materials are the preferred choice of materials for high temperature, wear resistance and high speed cutting applications because of their high melting points and remarkable hardness [1–3]. Al$_2$O$_3$-based ceramic matrix composites are widely used in wear, corrosive, and high temperature environments due to their excellent properties such as high hardness, chemical stability, excellent wear resistance, and high temperature oxidation resistance [4–6]. However, the wide applications of alumina are limited by their intrinsic brittleness. Hence, enough research has been devoted on ceramic materials to improve their flexural strength and fracture toughness in order to maximize their industrial applications [7–10]. Studies have indicated that the addition of 10 wt. % TiC as a reinforcement to the Al$_2$O$_3$ matrix can improve the hardness, fracture toughness, and thermal shock resistance of the composites [11,12]. In addition, introducing ductile reinforcement into the ceramic matrix may effectively improve both the ductility and toughness of the ceramic matrix composites.

Reports have shown that ductile metallic particles such as Ni, Fe, Al, Cu, Mo, and Nb have been added to the alumina matrix to improve its ductility [11–15]. Considerable efforts have been devoted to improve the mechanical properties of TiC-based cermets with Co as a binder. Although such efforts have shown some promise, this technique (of Co binder addition) exhibits several limitations, including high costs and environmental pollution [16,17]. Thus, researchers have been attempting to address these issues by replacing Co with other transition elements, such as Ni, Mo, and Ni-Mo. Ni is one of the prominent candidates as a binder, which can be widely utilized in various types of cermets [18,19]. The addition of transition and relatively soft material like Ni may have a significant influence in reducing the crack growth during the sintering process, due to its excellent oxidation resistance [20,21]. Furthermore, Ni as a binder is responsible for better toughness and ductility in the ceramic matrix composites [22,23]. Moreover, available literature shows that addition of Ni as binder in cermets can effectively improve the wear resistance of the composites [24–26].

Recent reports have demonstrated that the addition of Mo as binder in TiC-based cermets can improve its mechanical properties [27,28], which may be explained by the following mechanism: Mo increases the wettability between the binder and the ceramic phase by forming a Mo-rich shell around the TiC particles, which in turn helps in improving the properties of the cermets [29,30]. The mixing of additives with the matrix is generally carried out by manual mixing (hand mixing or agate mortar). However, mixing by mechanical milling (MM) has shown significant improvement in the strength and ductility of the composite materials due to the uniform distribution of the reinforcement/foreign particles [31–37]. Even though several studies have focused on the improvement of flexural strength and fracture toughness of the Al_2O_3-based ceramic composites, a systematic study dealing with the microstructural evolution and structure-property correlation is lacking. Therefore, this work focuses on the fabrication of Al_2O_3-TiC composites with different percentage of Ni and Nb addition (as additive) via MM combined with spark plasma sintering (SPS). The effect of additives content on the microstructure, hardness, and tribological properties of the composites was investigated in detail. The influence of both Ni and Nb addition on the relative density, hardness, and abrasive wear resistance is compared systematically.

2. Materials and Methods

Al_2O_3-10TiC composites were fabricated by SPS process using commercially available α-Al_2O_3 as matrix (from Alfa Aesar with 99.99% purity), with an average particle size of ~24 μm. TiC particles (from Alfa Aesar with 99.97% purity) with an average particle size of ~7 μm were used as the reinforcement (10 vol.%). In order to improve the bonding between the matrix and reinforcement, Ni & Nb additives (from Himedia, Mumbai, India, 99.99% purity), both with a particle size of ~3 μm, were added with different weight percentages (from 1 to 3 wt. %). The composite powder mixture was prepared by mechanical milling (MM) in a PM-400 planetary ball mill for 30 h in dry condition with a ball to powder ratio of 10:1 and at a set speed of 150 rpm. Phase analysis of the milled powders was carried out using powder diffraction technique with the help of X'Pert PRO PANalytical Diffractometer (from PANalytical, Kassel, Germany) with Cu-kα radiation (λ = 1.54184 Å), and the particle size was analyzed using the particle size analyzer (Malvern 2000, New Delhi, India), which is a laser based diffraction technique with water as dispersant. The particle morphologies were observed using field emission scanning electron microscope (FESEM) from JEOL (Freising, Germany) fitted with energy dispersive X-ray spectroscopy (EDX from Oxford Instruments plc, Oxfordshire, UK). The milled powders were loaded inside the SPS system (SPS Syntex, 725, New Delhi, India) with 15 mm diameter top and bottom punches. The sintering was carried out under vacuum with pressure less than 10^{-4} MPa. The composite powder was heated to 1673 K at a constant heating rate of 50 K/min and was held for 3 min at a pressure of 60 MPa.

After sintering, the samples were removed from the die to evaluate both the both physical and mechanical properties. The sintered samples were subjected to X-ray diffraction (XRD) after both the surfaces were ground to remove any residual graphite layer present in the sample. The density

of the sintered samples was measured using Archimedes principle. Microstructural observation was conducted using the optical microscope (OM from HITACHI, Feldkirchen, Germany) and FESEM. Hardness measurements were carried out using micro-indentation technique with the help of a computer-controlled LECO (AMH43 from LECO, Mönchengladbach, Germany) Vicker's microhardness tester. The micro-hardness device was equipped with a typical diamond indenter in the form of a pyramid with square base and an angle of 136° between the opposite faces. Indentations were carried out with an applied load of 1 g and a dwell time of 13 s. The abrasion test was performed using a high temperature abrasion tester—CM-9101 (according to ASTM G65 standards) at 873 K for 5 min cycling time under the applied load of 5 kg. These tests were carried out to analyze the weight loss and abrasion rate at given temperature and cycling time.

The CM-9101 abrasion tester set-up has a rotating metallic (Ni-based Inconel alloy) wheel of 100 mm diameter, which acts as a counter face against abrasive sample surface. The specimens were weighed initially on an electronic weighing machine, with an accuracy of 0.1 mg. They were then fixed in the specimen holder, which is located at one end of the lever, and the door was closed. The samples were heated to 873 K inside the chamber as per the working requirement of the cutting tool insert. 5 kg load was applied on the other end of the hydraulic arm with a rotation speed of 200 rpm, which is maintained by adjusting the knob. White alumina sand AFS 50/70 (with a hardness of 2000 Hv) as abrasive media was loaded in the hopper of the machine. The abrasive medium falls at a rate of 350 g/min between the specimen and the counter face during the entire run time of the experiment. The applied load presses the specimen against the counter face, while there is a continuous flow of abrasive medium between the specimen and the counter face. All the experiments were conducted for a constant time of 5 min. After completion of the experiment, the samples were again weighed and weight loss was recorded. The abrasion wear rate was calculated using the formula [38],

$$W_a = \left(\frac{\Delta G}{d} \right) \times M \times S \tag{1}$$

where W_a is the abrasion wear rate (mm^3/Nm), ΔG is mass loss (g), d is density (g/mm^3), M is the applied load (N), and S is the sliding distance (m) [39,40].

3. Results

3.1. Power Characterization

XRD patterns of the milled Al_2O_3-10TiC powder samples with and without the addition of binder are shown in Figure 1. The XRD patterns show the presence of only two phases with no new phases formed, indicating that no reaction has taken place between the matrix, reinforcement, and the binder during MM. In addition, the patterns do not show the presence of Ni/Nb peaks, which may be due to the low contents of Ni/Nb (<5 wt. %), which are below the detection limit of the XRD device. Hence, all the identified peaks correspond to the two phases Al_2O_3 and TiC. Figure 2a,c shows the FESEM micrograph of the Al_2O_3-10TiC milled powder (with 3 wt. % nickel) and their size distribution. It show two types of particles, big polygon-shaped Al_2O_3 particles (8–10 μm) and small equiaxed TiC particles (1–2 μm), distributed uniformly throughout the matrix. The presence of Ni/Nb was hard to identify due to the low amount of binder addition in the composite. Figure 2b,d reveals the Gaussian distribution function of the powder particles before and after MM. It shows that the particle size is reduced after MM and most of the particles fall between the range 1–10 μm after MM, as compared to 1–20 μm in the un-milled condition. The results are representative, since the size of the particles remain similar irrespective of the amount and type (Ni/Nb) of binder added and hence not shown here. This may be that Ni/Nb does not react with the matrix and/or the reinforcement. In addition, both these elements (Ni/Nb) have similar hardness levels (between 4.0 and 6.0) on Mohs scale.
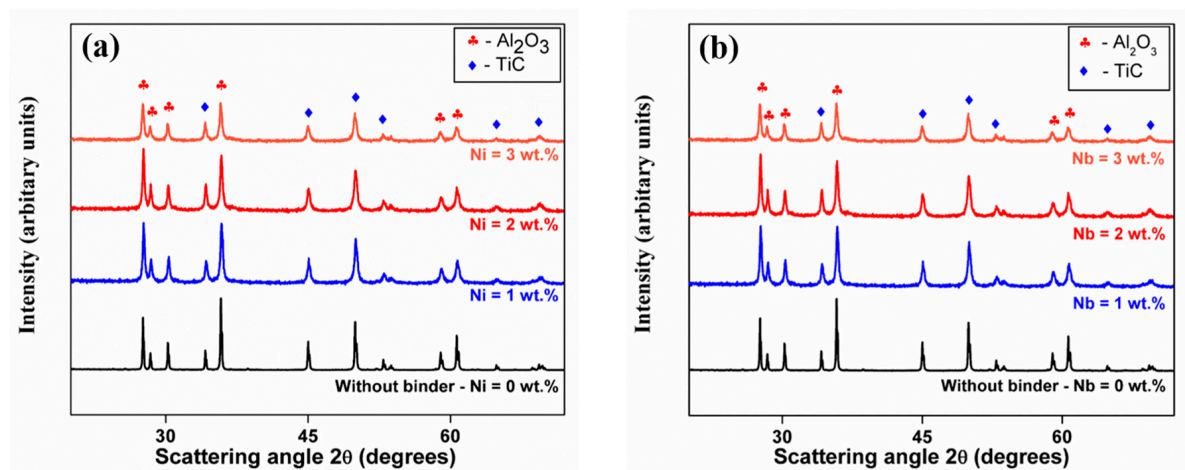
Figure 1. XRD (Cu-Kα) patterns of the Al$_2$O$_3$-10TiC-milled powder with the different binder content with (**a**) Ni and (**b**) Nb addition.
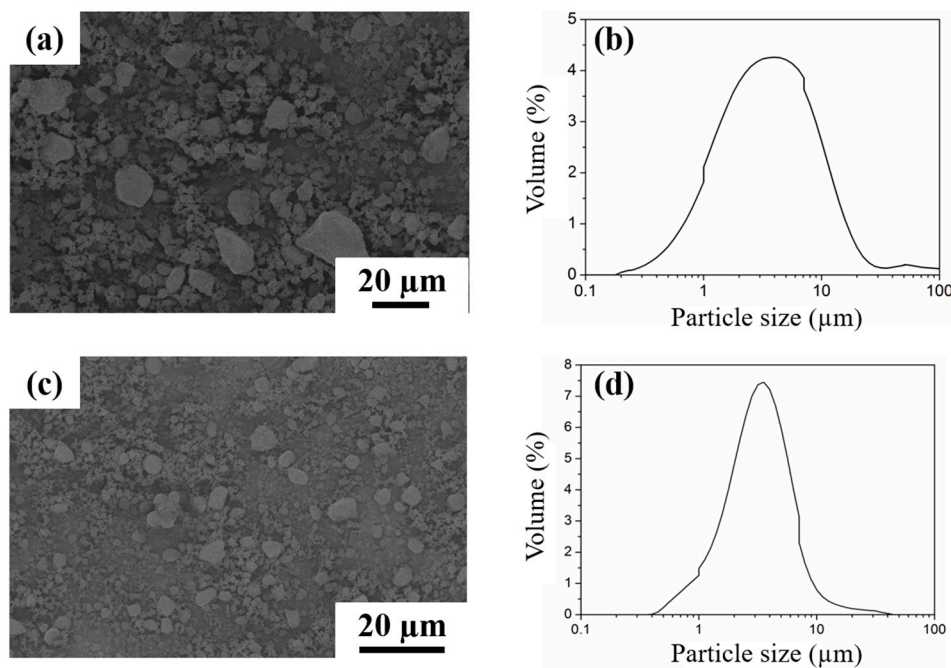

Figure 2. FESEM micrograph of Al$_2$O$_3$-10TiC powder with 3 wt. % Nb addition in (**a**) un-milled and (**c**) milled conditions along with their particle size distribution (**b**,**d**), respectively.

3.2. Microstructure and Mechanical Property of Bulk Sample

The FESEM micrographs of the bulk composite samples with and without the addition of different weight percentage (1–3 wt. %) binder (Ni/Nb) are shown in Figure 3a–g. The micrograph revels that the composite samples consist of two phases (bright and dark) distributed homogeneously in all the measured samples. It has been observed from the EDX analysis that the bright phase corresponds to TiC particles and the dark phases represents Al$_2$O$_3$ particles (see Figure 4). Traces of Ni/Nb are hard to be observed because of the low contents and the size of the particles. The micrographs does not show the presence of defects like porosity in the sample, suggesting these samples have a very high density. In addition, the microstructures also reveal the presence of an excellent interfacial bonding between the matrix (Al$_2$O$_3$) and the reinforcement (TiC) without the presence of any interfacial defects between the matrix and the reinforcement.
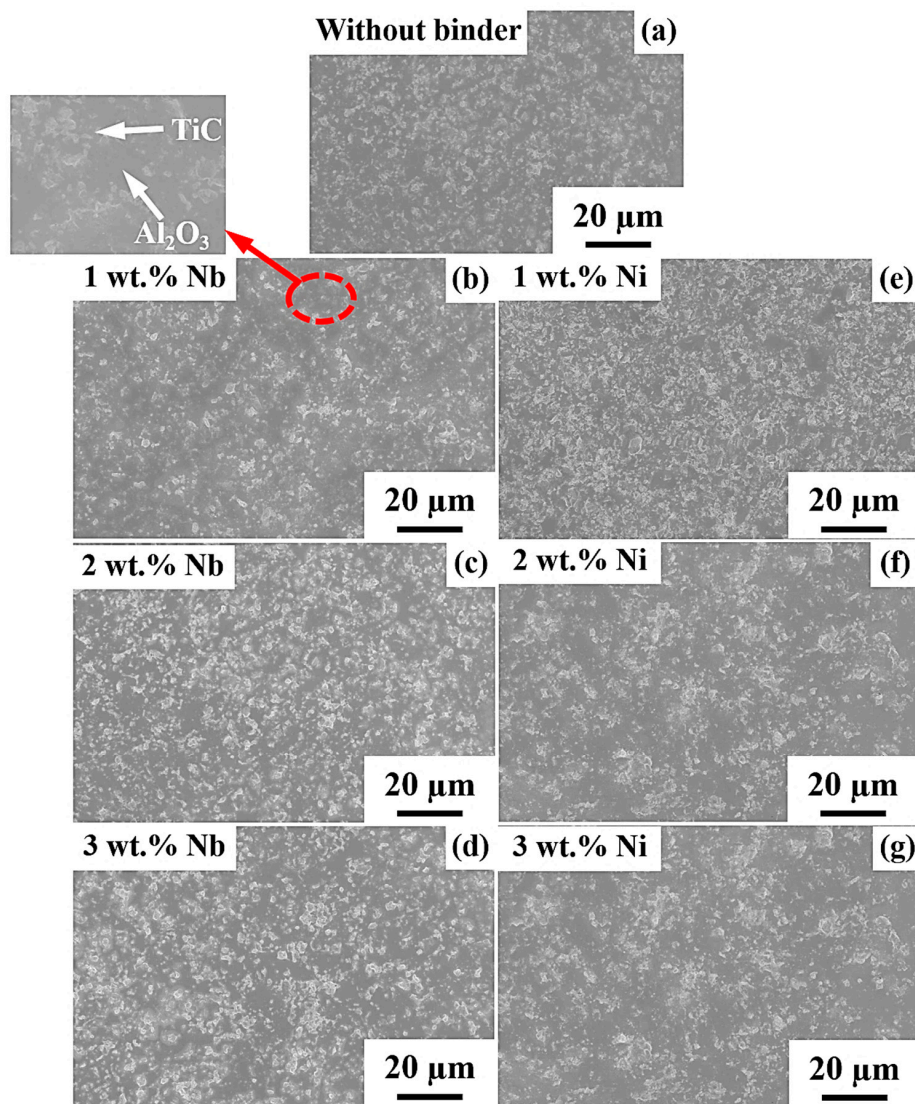
Figure 3. FESEM micrographs of the sintered Al_2O_3-TiC composite without binder (**a**) and with different contents (wt. %) of binder addition: Nb (**b**–**d**) and Ni (**e**–**g**).

The densification and hardness of the composites with the binder addition (Ni/Nb) are shown in Figure 5. The density of the composites increase from 3.9820 g/cc to 4.0713 g/cc, when the amount of Nb addition is increased from 1 wt. % to 2 wt. %, which amount to an increase in the relative density from ~96.5% to ~98%. The relative density shows a marginal decline (decreases to ~97.5%), when the Nb addition is increased to 3 wt. %. This marginal decrease in the relative density of the 3 wt. % Nb added composite may be attributed to the difference in wettability levels. Nb does not have a good wettability with the Al_2O_3 matrix as compared to Ni, and any increase in the Nb content beyond 2 wt. % does not help to improve the density of the Al_2O_3-10TiC composites. Similar trend is observed with the hardness data as well. The hardness levels of the composites increase with increasing addition of Nb from ~1410 MPa (without Nb addition) to ~1680 MPa for 1 wt. % addition of Nb. With further addition of Nb to 2 wt. %, the hardness on the composite increases to ~1870 MPa and then marginally decreases to 1770 MPa with 3 wt. % Nb addition. This decline in the hardness is attributed to the decrease in the relative density of the composite, which again is related to the wettability of Nb with Al_2O_3.

On the other hand, with the addition of Ni, both the density and the relative densities increase linearly. For instance, the relative density of the composites increases from ~96% (1 wt. % Ni addition) to ~96.5 wt. % (2 wt. % Ni) and finally to ~97% for 3 wt. % Ni addition. Similar trend has been observed also for the hardness values, where the hardness increases from ~1410 MPa without Ni addition to ~1625 MPa, ~1780 MPa, and ~1800 MPa for the addition of 1 wt. %, 2 wt. %, and 3 wt. % Ni, respectively. Such consistent increase in both relative densities and hardness of the composites with the addition of Ni is attributed to the complete wettability of Ni with the matrix Al_2O_3. It has been observed that the complete wettability provides better bonding strength with matrix and helps to reduce the amount of porosity, which results in the enhanced densities, flexural strength, and fracture toughness [41–43]. A highest hardness of ~1870 MPa is observed for the composites with 2 wt. % Nb addition and a least hardness of ~1625 MPa is observed for the composite with 1 wt. % Ni addition. In general, the samples with the addition of Nb shows better strength levels (hardness) than the composites with Ni addition. This may be attributed to the strength of Nb, which is slightly higher (Mohs scale 6.0) compared to Ni (Mohs scale 4.0).
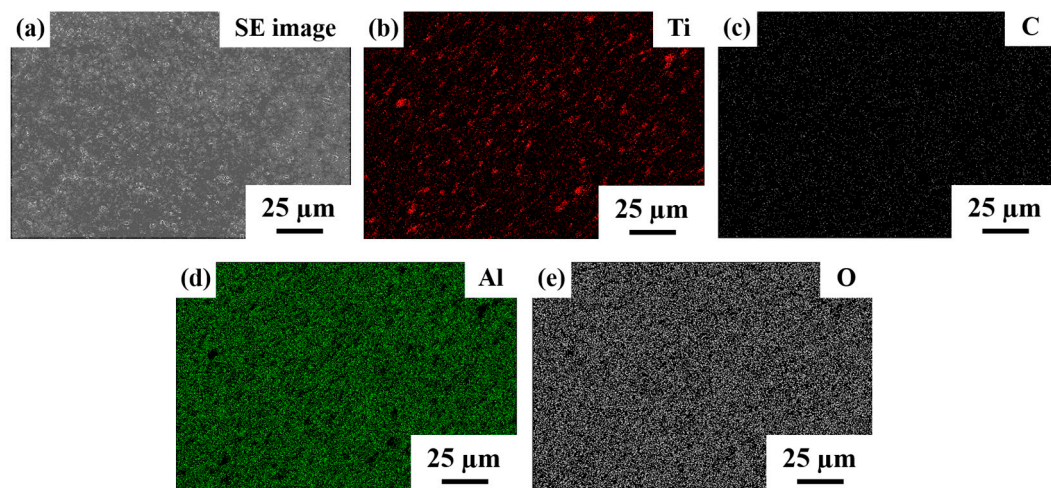

Figure 4. EDX mapping pf the sintered Al_2O_3-TiC composite without binder (**a**) secondary electron image, (**b**) Ti, (**c**) C, (**d**) Al, and (**e**) O phases.
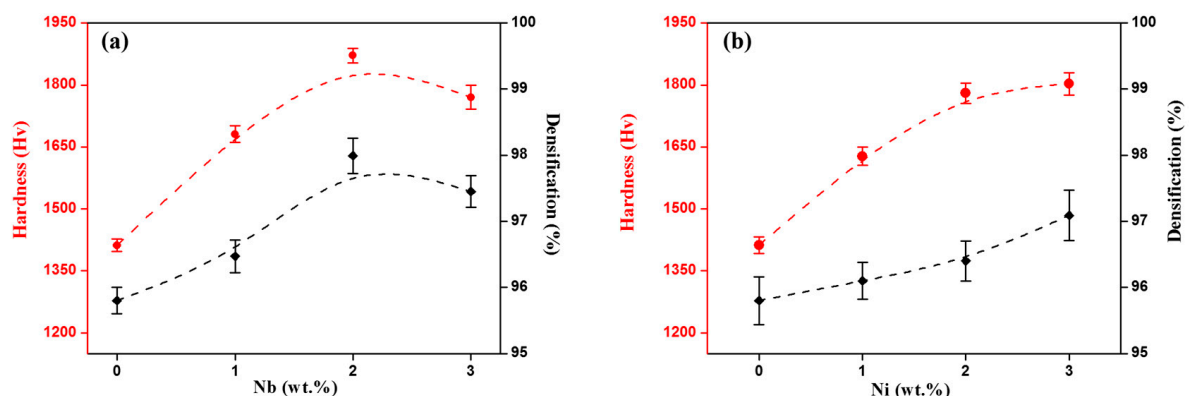

Figure 5. Densification and hardness plot of the Al_2O_3-TiC composite samples with different wt. % of (**a**) Nb and (**b**) Ni binder addition.

3.3. Abrasive Wear Study

Ceramic materials possess high hardness and relative low fracture toughness [44,45], and hence brittle micro-cutting wear mechanisms will predominate. However, sometimes plastic deformation

may also be observed during an abrasion wear process [46]. Figures 6 and 7 show the microstructure of the surfaces before and after abrasion test with the addition of Nb and Ni binders, respectively. Generally, from these images, it can be observed that the abrasive surfaces do not show any deep cutting mark, which is due to the presence of hard particles on the moving path of abradants. These hard particles are capable of resisting the abradant, resulting either in the rolling of abradants or the pulling out of particles themselves. Locally, some surfaces become uneven and even show the erosion of some fine particles. However, a uniform wear throughout the sample surface is observed in most of the samples. In the Nb added composites, some micro-cracks and detachment of the particles are observed in samples especially at higher amounts of Nb (3 wt. % Nb) addition, as marked by arrows in the Figure 6h. However, the presence of micro-cracks and detachment of particles is comparatively less in the samples with 1 wt. % and 2 wt. % addition of Nb. This effect is attributed to the decrease in the relative density and, in turn, hardness in the composites with 3 wt. % Nb addition, compared to the other two samples with 1 wt. % and 2 wt. % Nb addition, respectively. In case of the composites with Ni as binder, samples surface changes show a uniform trend, which is in accordance with the increase in the addition of Ni content.
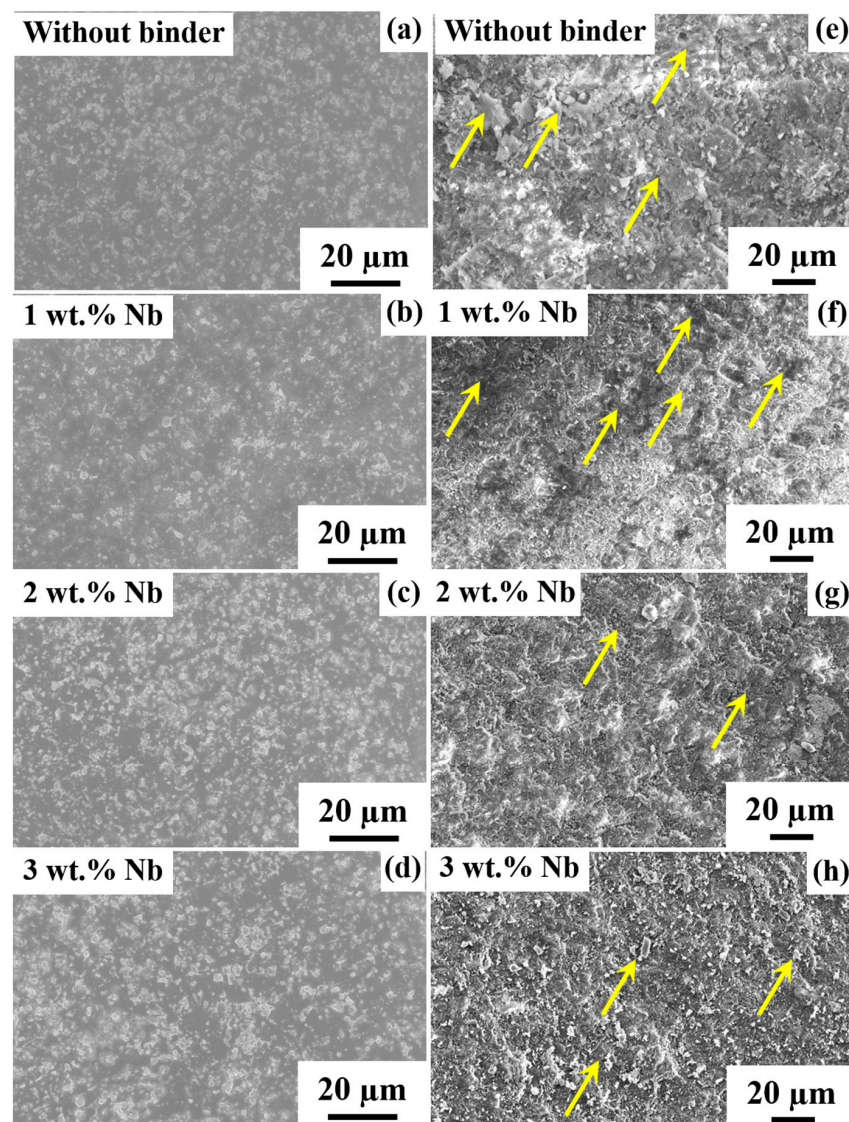

Figure 6. FESEM micrographs of the Al$_2$O$_3$-10TiC composite samples without Nb and with different contents of Nb (**a–d**) before and (**e–h**) after abrasion test.
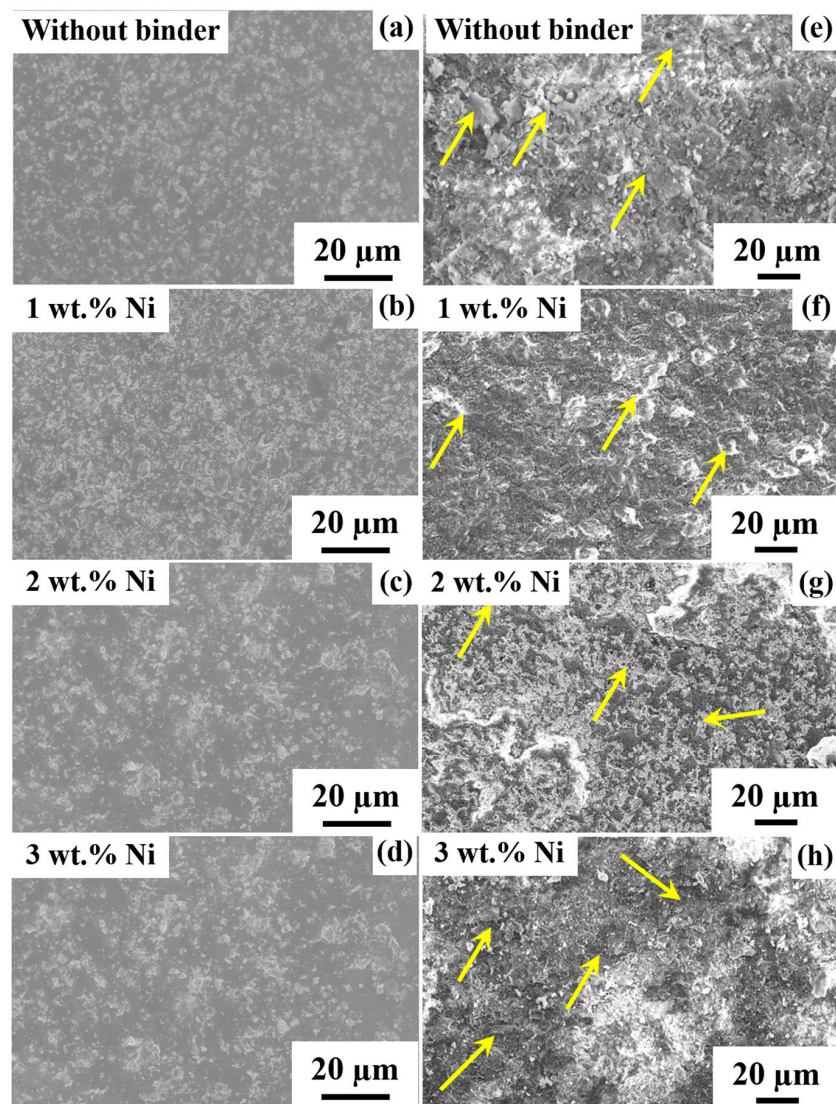
Figure 7. FESEM micrographs of the Al_2O_3-10TiC composite samples without Ni and with different contents of Ni (**a**–**d**) before and (**e**–**h**) after abrasion test.

The weight loss and the wear rate data of the composites with the addition of Nb and Ni are shown in Figure 8. Both the weight loss and wear rate data show that the addition of both Nb and Ni in general improves the wear resistance of the material, due to improved relative densities and, in turn, the hardness of the composites. However, the lone exception is the composite sample with 3 wt. % Nb addition, where weight loss increases compared to the sample with 2 wt. % Nb addition, suggestion poor wear resistance. The results are in compliance with the FESEM images and also with the relative density and hardness data. From these experimental data, the following observations can be made: both the hardness (strength) and the wear resistance increases with increase in the Nb addition until 2 wt. %. Addition of Nb content beyond 2 wt. % decreases both the hardness and wear resistance, due to issues with the wettability, and hence there is a decrease in the relative density of the composites. However, with the addition of Ni, both the hardness and wear resistance increases with increase in the Ni content. In general, the hardness and wear resistance of the composites are superior when Nb is added as a binder rather than Ni. This may be attributed to the marginal increase in hardness of Nb compared to Ni.
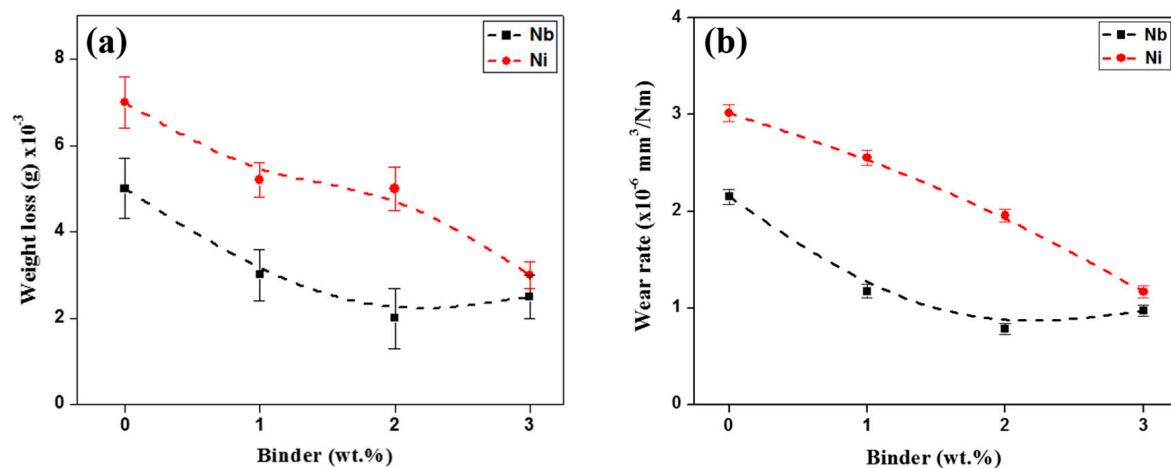
Figure 8. Plots showing the effect of Nb and Ni binder on the (**a**) weight loss and (**b**) abrasion rate on Al_2O_3-10TiC composite samples.

4. Summary

Al_2O_3-10TiC bulk ceramic matrix composites were successfully prepared by powder metallurgical route (mechanical milling combined with spark plasma sintering) with the addition of Ni/Nb as metallic additives.

- ➢ XRD data shows the presence of two phases Al_2O_3 and TiC, confirming no reaction between the matrix, reinforcement, and metallic binders during the mechanical milling and subsequent spark plasma sintering processes. However, no peaks of Ni/Nb are observed owing to the small amounts of Ni/Nb addition, which is below the deductible limits of the XRD setup.
- ➢ The microstructure of the composite reveals homogeneous distribution of the TiC particles within the Al_2O_3 matrix. The relative density, hardness, and the wear resistance of the composites increase with the addition of Nb until 2 wt. %. Any addition of Nb beyond 2 wt. % (3 wt. % addition of Nb) hampers their properties, due to relatively poor wettability of Nb with the Al_2O_3 matrix. Nevertheless, the properties of composites with 3 wt. % addition of Nb are better than the samples without the addition of Nb.
- ➢ On the other hand, with the addition of Ni, the relative density, hardness, and wear resistance increases with increase in the Ni content. In general, the samples with the addition of Nb as binder show more improved properties than the composites with Ni addition, which is attributed to the marginal increase in the hardness of Nb compared to Ni.
- ➢ Overall results show that the addition of metallic binders improve the relative density, hardness, and wear resistance of the Al_2O_3-10TiC composite samples.

Author Contributions: A.K.C. and K.G.P. formulated the idea. R.K. and T.M. helped with the literature survey. R.K. and A.K.C. carried out the experiments. R.K. and T.M. wrote the paper, and both A.K.C. and K.G.P. supervised the research. The authors would like to thank NTNUs open access policy that motivated to publish in an open access journal.

Conflicts of Interest: The authors declare no conflict of interest.

References

1. Ruehle, M.; Evans, A.G. High toughness ceramics and ceramic composites. *Prog. Mater. Sci.* **1989**, *33*, 85–167. [CrossRef]

2. Moya, J.S.; Lopez-Esteban, S.; Pecharroman, C. The challenge of ceramic/metal microcomposites and nanocomposites. *Prog. Mater. Sci.* **2007**, *52*, 1017–1090. [CrossRef]

3. Mayrhofer, P.H.; Mitterer, C.; Hultman, L.; Clemens, H. Microstructural design of hard coatings. *Prog. Mater. Sci.* **2006**, *51*, 1032–1114. [CrossRef]

4. Zhao, J.; Yuan, X.L.; Zhou, Y.H. Cutting performance and failure mechanisms of an Al_2O_3/WC/TiC micro–nano-composite ceramic tool. *Int. J. Refract. Met. Hard Mater.* **2010**, *28*, 330–337. [CrossRef]

5. Liu, C.; Zhang, J.; Sun, J.; Zhang, X. Tribological properties of pressureless sintered alumina matrix ceramic materials improved by diopside. *J. Eur. Ceram. Soc.* **2008**, *28*, 199–204. [CrossRef]

6. Meybodi, S.M.; Bafrooei, H.B.; Ebadzadeh, T.; Tazike, M. Microstructure and mechanical properties of Al_2O_3–20 wt% Al_2TiO_5 composite prepared from alumina and titania nano powders. *Ceram. Int.* **2013**, *39*, 977–982. [CrossRef]

7. Chaubey, A.K.; Prashanth, K.G.; Ray, N.; Wang, Z. Study on in-situ synthesis of Al-TiC composite by self propagating high temperature synthesis process. *Mater. Sci. Indian J.* **2015**, *12*, 454–461.

8. Acchar, W.; Silva, Y.B.F.; Cairo, C.A. Mechanical properties of hot-pressed ZrO_2 reinforced with (W, Ti)C and Al_2O_3 additions. *Mater. Sci. Eng. A* **2010**, *527*, 480–484. [CrossRef]

9. Xu, L.; Huang, C.; Liu, H.L.; Zou, B.; Zhu, H.; Zhao, G.; Wang, J. Study on in-situ synthesis of ZrB_2 whiskers in ZrB_2–ZrC matrix powder for ceramic cutting tools. *Int. J. Refract. Met. Hard Mater.* **2013**, *37*, 98–105. [CrossRef]

10. Sktani, Z.D.I.; Azhar, A.Z.A.; Ratnam, M.M.; Ahmad, Z.A. The influence of in-situ formation of hibonite on the properties of zirconia toughened alumina (ZTA) composites. *Ceram. Int.* **2014**, *40*, 6211–6217. [CrossRef]

11. Gong, J.; Miao, H.; Zhao, Z. The influence of TiC-particle-size on the fracture toughness of Al_2O_3–30 wt. % TiC composites. *J. Eur. Ceram. Soc.* **2001**, *21*, 2377–2381. [CrossRef]

12. Xing, Y.; Deng, J.; Zhao, J.; Zhang, G.; Zhang, K. Cutting performance and wear mechanism of nanoscale and microscale textured Al_2O_3/TiC ceramic tools in dry cutting of hardened steel. *Int. J. Refract. Met. Hard Mater.* **2014**, *43*, 46–58. [CrossRef]

13. Wang, H.; Wang, B.; Li, S.; Xue, Q.; Huang, F. Toughening magnetron sputtered TiB_2 coatings by Ni addition. *Surf. Coat. Technol.* **2013**, *232*, 767–774. [CrossRef]

14. Zawrah, M.F.; Abdel-kader, H.; Elbaly, N.E. Fabrication of Al_2O_3–20 vol.% Al nanocomposite powders using high energy milling and their sinterability. *Mater. Res. Bull.* **2012**, *47*, 655–661. [CrossRef]

15. Sun, X.; Han, W.; Hu, P.; Wang, Z.; Zhang, X. Microstructure and mechanical properties of ZrB_2–Nb composite. *Int. J. Refract. Met. Hard Mater.* **2010**, *28*, 472–474. [CrossRef]

16. Mohammadpour, M.; Abachi, P.; Pourazarang, K. Effect of cobalt replacement by nickel on functionally graded cemented carbonitrides. *Int. J. Refract. Met. Hard Mater.* **2012**, *30*, 42–47. [CrossRef]

17. Song, W.; Hu, J.; Zhao, Y.; Shao, D.; Li, J. Efficient removal of cobalt from aqueous solution using β-cyclodextrin modified graphene oxide. *RSC Adv.* **2013**, *3*, 9514–9521. [CrossRef]

18. Tucker, M.C.; Cheng, L.; DeJonghe, L.C. Inorganic binder-containing composite cathode contact materials for solid oxide fuel cells. *J. Power Sourc.* **2013**, *224*, 174–179. [CrossRef]

19. Kakade, M.B.; Ramanathan, S.; Das, D. Gel-combustion, characterization and processing of porous Ni–YSZ cermet for anodes of solid oxide fuel cells (SOFCs). *Ceram. Int.* **2011**, *37*, 195–200. [CrossRef]

20. Kumar, B.V.M.; Kumar, J.R.; Basu, B. Crater wear mechanisms of TiCN–Ni–WC cermets during dry machining. *Int. J. Refract. Met. Hard Mater.* **2007**, *25*, 392–399. [CrossRef]

21. Özer, A.; Kriven, W.M.; Tür, Y.K. The effect of 3 mol.% Y_2O_3 stabilized ZrO_2 produced by a steric entrapment method on the mechanical and sintering properties of Cr_3C_2 based cermets. *Mater. Sci. Eng. A* **2012**, *556*, 878–884. [CrossRef]

22. Yang, F.; Guo, Z.M.; Hao, J.J.; Shi, Y.L. Self-Propagating High-Temperature Synthesis of TiB_2-Ti(C,N) Cermets Composite Powder. *Adv. Mater. Res.* **2012**, *468*, 1247–1250. [CrossRef]

23. Saidi, A.; Barati, M. Production of (W, Ti)C reinforced Ni–Ti matrix composites. *J. Mater. Process. Technol.* **2002**, *124*, 166–170. [CrossRef]

24. Hussainova, I. Effect of microstructure on the erosive wear of titanium carbide-based cermets. *Wear* **2003**, *255*, 121–128. [CrossRef]

25. Rodriguez-Barrero, S.; Fernandez-Larrinoa, J.; Azkona, I.; Lopez de Lacalle, L.N.; Polvorosa, R. Enhanced performance of nanostructured coatings for drilling by droplet elimination. *Mater. Manuf. Process.* **2016**, *31*, 593–602. [CrossRef]

26. Polvorosa, R.; Suarez, A.; Lopez de Lacalle, L.N.; Cerrillo, I.; Wertland, A.; Veiga, F. Tool wear on nickel alloys with different coolant pressures: Comparison of Alloy 718 and Waspaloy. *J. Manuf. Process.* **2017**, *26*, 44–56. [CrossRef]

27. Li, Y.; Liu, N.; Zhang, X.; Rong, C. Effect of Mo addition on the microstructure and mechanical properties of ultra-fine grade TiC–TiN–WC–Mo$_2$C–Co cermets. *Int. J. Refract. Met. Hard Mater.* **2008**, *26*, 190–196. [CrossRef]

28. Guo, X.; Niu, Y.; Huang, L.; Ji, H.; Zheng, X. Microstructure and Tribological Property of TiC-Mo Composite Coating Prepared by Vacuum Plasma Spraying. *J. Therm. Spray Technol.* **2012**, *21*, 1083–1090. [CrossRef]

29. Wang, Y.; Shu, S.; Qiu, F.; Zhou, D.; Wang, J.; Jiang, Q. Effect of W content on the compression properties and abrasive wear behavior of the (TiB2–TiCxNy)/(Ni + W) composites. *Mater. Des.* **2013**, *45*, 286–291. [CrossRef]

30. Chen, X.; Xiong, W.; Qu, J.; Yang, Q.; Yao, Z.; Huang, Y. Microstructure and mechanical properties of (Ti, W, Ta)C-xMo-Ni cermets. *Int. J. Refract. Met. Hard Mater.* **2012**, *31*, 56–61. [CrossRef]

31. Chaubey, A.K.; Scudino, S.; Mukhopadhyay, N.K.; Khoshkhoo, M.S.; Mishra, B.K.; Eckert, J. Effect of particle dispersion on the mechanical behavior of Al-based metal matrix composites reinforced with nanocrystalline Al–Ca intermetallics. *J. Alloys Compd.* **2012**, *536*, 134–137. [CrossRef]

32. Wang, Z.; Prashanth, K.G.; Scudino, S.; Chaubey, A.K.; Sordelet, D.J.; Zhang, W.W.; Li, Y.Y.; Eckert, J. Tensile properties of Al matrix composites reinforced with in situ devitrified Al$_{84}$Gd$_6$Ni$_7$Co$_3$ glassy particles. *J. Alloys Compd.* **2014**, *589*, 419–422. [CrossRef]

33. Prashanth, K.G.; Scudino, S.; Surreddi, K.B.; Sakaliysla, M.; Murty, B.S.; Eckert, J. Crystallization of Zr$_{65}$Ag$_5$Cu$_{12.5}$Ni$_{10}$Al$_{7.5}$ glassy powders produced by ball milling of pre-alloyed ingots. *Mater. Sci. Eng. A* **2009**, *513–514*, 279–285. [CrossRef]

34. Wang, Z.; Tan, J.; Sun, B.A.; Scudino, S.; Prashanth, K.G.; Zhang, W.W.; Li, Y.Y.; Eckert, J. Fabrication and mechanical properties of Al-based matrix composites reinforced with Mg$_{65}$Cu$_{20}$Zn$_5$Y$_{10}$ metallic glass particles. *Mater Sci. Eng. A* **2014**, *600*, 53–58. [CrossRef]

35. Prashanth, K.G.; Kumar, S.; Scudino, S.; Murty, B.S.; Eckert, J. Fabrication and response of Al$_{70}$Y$_{16}$Ni$_{10}$Co$_4$ glass reinforced metal matrix composites. *Mater. Manuf. Proc.* **2011**, *26*, 1242–1247. [CrossRef]

36. Prashanth, K.G.; Murty, B.S. Production, kinetic study and properties of Fe-based glass and its composites. *Mater. Manuf. Proc.* **2010**, *25*, 592–597. [CrossRef]

37. Wang, Z.; Tan, J.; Scudino, S.; Sun, B.A.; Qu, R.T.; He, J.; Prashanth, K.G.; Zhang, W.W.; Li, Y.Y.; Eckert, J. Mechanical behavior of Al-based matrix composites reinforced with Mg$_{58}$Cu$_{28.5}$Gd$_{11}$Ag$_{2.5}$ metallic glass. *Adv. Powder Technol.* **2014**, *25*, 635–639. [CrossRef]

38. Radhika, N.; Raghu, R. Three body abrasion wear behaviour of functionally graded aluminium/B$_4$C metal matrix composite using design of experiments. *Proc. Eng.* **2014**, *97*, 713–722. [CrossRef]

39. Prashanth, K.G.; Scudino, S.; Chaubey, A.K.; Loeber, L.; Wang, P.; Attar, H.; Schimansky, F.; Pyczak, F.; Eckert, J. Processing of Al-12Si–TNM composites by selective laser melting and evaluation of compressive and wear properties. *J. Mater. Res.* **2016**, *31*, 55–65. [CrossRef]

40. Ehtemam-Haghighi, S.; Prashanth, K.G.; Attar, H.; Chaubey, A.K.; Cao, G.C.; Zhang, L.-C. Evaluation of mechanical and wear properties of Ti-xNb-7Fe designed for biomedical applications. *Mater. Des.* **2016**, *111*, 592–599. [CrossRef]

41. Murthy, T.S.; Subramanian, C.; Fotedar, R.K.; Gonal, M.R.; Sengupta, P.; Kumar, S.; Suri, A.K. Preparation and property evaluation of TiB$_2$ + TiSi$_2$ composite. *Int. J. Refract. Met. Hard Mater.* **2009**, *27*, 629–636. [CrossRef]

42. Kumar, R.; Chaubey, A.K.; Bathula, S.; Jha, B.B.; Dhar, A. Synthesis and characterization of Al$_2$O$_3$-TiC nano-composite by spark plasma sintering. *Int. J. Refract. Met. Hard Mater.* **2016**, *54*, 304–308. [CrossRef]

43. Wang, Z.; Georgarakis, K.; Zhang, W.W.; Prashanth, K.G.; Eckert, J.; Scudino, S. Reciprocating sliding wear behavior of high-strength nanocrystalline AL84Ni7Gd6Co3 alloys. *Wear* **2017**, *383*, 78–84. [CrossRef]

44. Wang, Z.; Qu, R.T.; Scudino, S.; Sun, B.A.; Prashanth, K.G.; Louzguine-Luzgin, D.V.; Chen, M.W.; Zhang, Z.F.; Eckert, J. Hybrid nanostructured aluminum alloys with high strength. *NPG Asia Mater.* **2015**, *7*, e229. [CrossRef]

45.　Suryawanshi, J.; Prashanth, K.G.; Scudino, S.; Eckert, J.; Prakash, O.; Ramamurty, U. Simultaneous enhancements of strength and toughness in an Al-12Si alloy synthesized using selective laser melting. *Acta Mater.* **2016**, *115*, 285–294. [CrossRef]

46.　Mao, D.S.; Li, J.; Guo, S.Y.; Mao, Z.Y. Study of abrasion behavior of an advanced Al_2O_3-TiC-Co ceramic. *Wear* **1997**, *209*, 153–159. [CrossRef]